The Mechanism of β-Hematin Formation in Acetate Solution. Parallels between Hemozoin Formation and Biomineralization Processes†

Timothy J. Egan,* Winile W. Mavuso, and Kanyile K. Ncokazi

Department of Chemistry, University of Cape Town, Private Bag, Rondebosch 7701, South Africa

Received June 13, 2000; Revised Manuscript Received October 19, 2000

ABSTRACT: Formation of β-hematin in acidic acetate solution has been investigated using quantitative infrared spectroscopy, X-ray diffraction, and scanning and transmission electron microscopy. The process occurs via rapid precipitation of amorphous (or possibly nanocrystalline) hematin, followed by slow conversion to crystalline β-hematin. Definitive evidence that the reaction occurs during incubation in acetate medium, rather than during the drying stage, is provided by X-ray diffraction and infrared spectroscopy of the wet material. The reaction follows a sigmoidal function indicative of a process of nucleation and growth and was modeled using the Avrami equation. Reaction rates and the dimensionality of growth (as indicated by the value of the Avrami constant) are strongly influenced by stirring rate. The reaction follows Arrhenius behavior, and there is a strong dependence of both the rate constant and the Avrami constant on acetate concentration. Acetate may act as a phase transfer catalyst, solubilizing hematin and facilitating its redeposition as β-hematin. The pH dependence of the process indicates that only the monoprotonated species of hematin is active in forming β-hematin. The formation of β-hematin closely parallels many mineralization processes, and this suggests that hemozoin formation may be a unique biomineralization process. Inferences are drawn with respect to the formation of hemozoin in vivo.

Malaria is a leading cause of mortality and morbidity in tropical regions, especially in Africa, and contributes significantly to economic underdevelopment (*1*). Investigations of the biology and chemistry of the malaria parasite are thus of considerable interest.

During its blood stage, the malaria parasite proteolyzes host hemoglobin in an acidic vacuole to obtain amino acids (*2*), releasing heme as a byproduct which is autoxidized to potentially toxic (*3*) hematin [aquaferriprotoporphyrin IX, H_2O-Fe(III)PPIX].[1] It detoxifies this hematin, at least in part, by conversion to a highly insoluble substance known as hemozoin (malaria pigment) (*4*). X-ray diffraction has unequivocally shown that this material is structurally and chemically identical to a synthetic Fe(III)PPIX product known as β-hematin (*5*). Current evidence indicates that quinoline-based antimalarials, active against the blood stage of the disease, block the detoxification of Fe(III)PPIX (*6*−*12*), probably at least partly by inhibiting β-hematin formation (*11*−*19*).

Recently, determination of the structure of β-hematin (*20*) has demonstrated that it is a crystalline cyclic dimer of Fe(III)PPIX which involves reciprocal coordination of the ionized heme-propionate side chain of one Fe(III)PPIX to the Fe(III) center of the other. These dimer units interact in the crystal via intermolecular forces that include hydrogen bonding through the remaining un-ionized heme propionic acid group on each Fe(III)PPIX. This material is not a polymer as previously believed, and the language and concepts of polymerization are not appropriate to understanding its formation.

The mechanism of β-hematin formation in vivo or in vitro is still not clear. A number of proposals have been put forward for the process in vivo, with suggestions that it is enzyme-catalyzed (*13*), spontaneous (*14*), autocatalytic (*15*), lipid-catalyzed (*21*, *22*), or catalyzed or initiated by histidine-rich proteins (*16*, *19*, *23*). Synthesis of β-hematin in vitro is usually carried out either in aqueous acetate solution from hematin [H_2O-Fe(III)PPIX] (*14*, *15*, *21*, *24*−*26*) or in dry methanol using hemin [Cl-Fe(III)PPIX] and the organic base 2,6-lutidine (*5*, *27*). There have been a few studies in which the rate of β-hematin formation in acetate solution has been reported (*13*, *21*, *26*, *28*, *29*), but no systematic investigation of the time-course of formation appears to have been undertaken, and only a limited set of conditions has been investigated. In a number of other studies, the conditions have been varied, but the extent of β-hematin formation has been reported at fixed reaction times only (*14*, *21*, *30*, *31*). As a result, there is considerable confusion over the rate at which the product forms and over whether it forms at all under certain conditions (*14*, *29*−*33*). In only one case has a direct spectroscopic method been employed to monitor the course of reaction (*29*).

Understanding the chemical mechanism of β-hematin formation is a prerequisite for understanding hemozoin formation in vivo. For that reason, we have undertaken a

†This work was supported by the National Research Foundation of South Africa and the University Research Committee of the University of Cape Town.

* To whom correspondence should be addressed at the Department of Chemistry, University of Cape Town, Private Bag, Rondebosch 7701, South Africa. Tel.: +27-21-650-2528; Fax: +27-21-689-7499; E-mail: tegan@psipsy.uct.ac.za.

[1] Abbreviations: Fe(III)PPIX, ferriprotoporphyrin IX; HRPII, histidine-rich protein II; SEM, scanning electron microscopy; TEM, transmission electron microscopy; XRD, X-ray diffraction.

10.1021/bi0013501 CCC: $20.00
Published on Web 12/07/2000

detailed investigation of synthetic β-hematin formation in acetate solution using infrared (IR) spectroscopy, X-ray diffraction analysis (XRD), and both scanning and transmission electron microscopy (SEM and TEM).

MATERIALS AND METHODS

Materials. All materials used were of analytical grade, or of the highest grade of purity available from commercial suppliers. Stock solutions of acetate (12.8 M) were prepared by carefully adding a saturated solution of sodium hydroxide to 365 mL of glacial acetic acid with continuous stirring, avoiding precipitation of sodium acetate throughout the process. The pH was monitored, and when the volume of the mixture was close to 500 mL, it was adjusted to 5.0 (except where otherwise indicated). The solution was then made up to 500 mL with deionized water. Upon dilution to 4.5 M in the final reaction mixture, the pH is found to decrease to 4.5. For other final acetate concentrations or other final pH values, the 12.8 M acetate stock solution was prepared at appropriate pH values to give the correct pH in the reaction mixture. In each case, the final reaction mixture pH was checked and found to be correct to within 0.05 pH unit.

Reaction Vessel. Reactions were carried out in a 100 mL jacketed glass titration cell with an internal diameter of 33 mm, and the temperature was controlled to within 0.5 °C using a thermostated water bath. The mixture was stirred with a magnetic stirrer using a stirrer bar 20 mm in length and 5 mm in diameter. Except for specifically mentioned experiments which were unstirred or stirred at half-speed, the reaction mixture was stirred at an estimated 150 ± 10 rpm.

Reaction Conditions and Effect of Temperature. For the initial studies at 60 °C and those on the effect of temperature on reaction rate, a final acetate concentration of 4.5 M and a pH of 4.5 were used. In each case, 75 mg of hemin (bovine, Sigma) was dissolved in 14.5 mL of 0.100 M NaOH. This solution was immediately placed in the titration cell preset at the appropriate temperature (60, 50, 37, or 30 °C). Within 10 min, 1.45 mL of 1.00 M HCl was added to this solution in order to neutralize the NaOH. Throughout the procedure, a lid was used to prevent evaporation from the reaction vessel. After a further 3−5 min of temperature equilibration, 8.825 mL of stock acetate solution (preequilibrated at the reaction temperature) was added to the titration cell. Samples (1.8 mL) of the suspension were withdrawn at predetermined time intervals and quenched on ice. All samples were washed with about 65 mL of deionized water, filtered using 0.22 μm cellulose nitrate filtration disks, and dried at room temperature for at least 48 h over silica gel and P_2O_5 (except where otherwise indicated). One set of experiments was carried out at 60 °C, but at an estimated stirring rate of 75 ± 10 rpm, while another was carried out unstirred under the same conditions. Where the reaction was performed unstirred, the mixture was briefly agitated before withdrawal of samples in order to obtain a homogeneous suspension.

Effect of Acetate Concentration. Studies on the effect of acetate concentration were carried out as described above, except that stock acetate solutions were prepared so as to give the same final pH (4.5) in each reaction mixture. Where concentrations of acetate exceeded 4.5 M, the volume of NaOH solution used to dissolve the hemin was reduced so that the final total volume remained constant in all experiments. These experiments were all performed at 60 °C. A trial run was carried out at the beginning of each study to determine the sampling interval for that particular run.

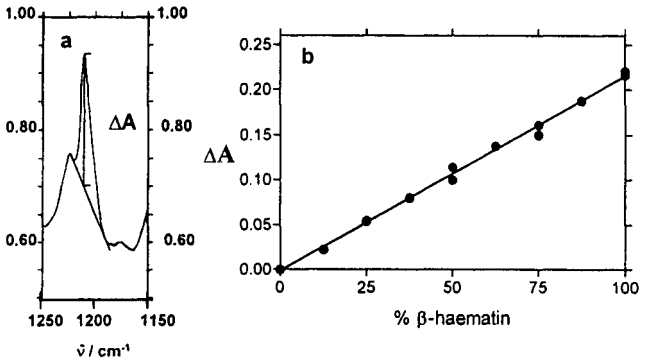

FIGURE 1: Typical infrared absorbance spectrum (a) of a sample obtained during β-hematin formation showing how the difference absorbance readings were obtained from the spectrum. Absolute absorbance readings (as opposed to ΔA values) differ from sample to sample because of changes in the baseline absorbance from one KBr disk to another. Calibration plot (b) showing ΔA_{1210} as a function of β-hematin percentage in samples made up by mixing known masses of hematin and β-hematin.

Effect of pH. The effect of pH on reaction kinetics was investigated exactly as described above, except that the pH of the acetate stock solutions was adjusted so as to give the correct final pH in the reaction mixture (2.5, 3.0, 3.5, 4.0, or 5.0). This was achieved by mixing appropriate ratios of 12.8 M acetate solution (pH 5.0) with 12.8 M acetic acid solution (for final pH below 4.5) or by using more concentrated NaOH in the starting hemin solution (for a final pH of 5.0 in the reaction mixture). In all cases, the total acetate concentration was 4.5 M, and the temperature was fixed at 60 °C.

Effect of Seeding. The effect of seeding on reaction rate was investigated in 4.5 M acetate at pH 4.5 and 50 °C and in 8.5 M acetate at pH 4.5 and 60 °C. The procedure used was the same as that described above except that 7.5 mg (10% seeding) or 37.5 mg (50% seeding) of β-hematin was added to the reaction mixture immediately following neutralization of NaOH with HCl, but prior to addition of the acetate solution.

Infrared Spectroscopy. Infrared spectroscopy was the primary method used to monitor the reaction kinetics. In each case, after drying, 1.53 ± 0.01 mg of sample, weighed out using a six-place balance, was ground together with 200 ± 1 mg of KBr with an agate mortar and pestle and compressed under 10 ton pressure for 1 min to produce a disk of 16 mm diameter. Infrared spectra were collected between 1250 and 1150 cm^{-1} in the absorbance mode using a Perkin-Elmer 983 infrared spectrometer. Growth of the β-hematin peak at 1210 cm^{-1} from the shoulder of the peak at 1229 cm^{-1} was monitored. A difference absorbance reading for each sample was measured as shown in Figure 1a. A calibration plot was prepared by mixing well-characterized (*32*) samples of hematin and β-hematin in known mass proportions (Figure 1b). Strictly ΔA_{1210} should show a linear dependence on the mole fraction of β-hematin rather than mass fraction, but as the molar masses of hematin and β-hematin differ by only 2.9% per equivalent of Fe(III)PPIX, these are experimentally

indistinguishable in the current system. As a result, the mass fraction of hematin can be approximated by eq 1:

$$m/m_0 \approx 1 - \Delta A/\Delta A_\infty \quad (1)$$

where m is the mass of hematin remaining in the sample, m_0 is the initial mass of hematin in the sample, ΔA is the difference absorbance at 1210 cm^{-1} due to β-hematin, and $\Delta A_\infty$is the final difference absorbance at the end of the reaction.

X-ray Diffraction and Electron Microscopy. For X-ray powder diffraction determinations, the samples were prepared using much larger quantities of reactants (200 mg of hemin used in each experiment and all volumes scaled up accordingly). In each case, the reaction was allowed to proceed for a specified time period; then the entire sample was quenched on ice, filtered, and washed. A separate experiment was thus carried out for each time point. After drying, the samples were finely ground to preclude preferred orientation effects, and the powder diffraction patterns were collected on the entire sample using a Philips PW1050/80 vertical goniometer in the 2θ range 5−40° with Co Kα radiation (λ = 1.789 Å) or Cu Kα radiation (λ = 1.541 Å), as indicated, in aluminum sample holders. In a few experiments, the sample was not dried, and the diffraction patterns were obtained on the wet material.

Scanning and transmission electron microscopy was carried out by the University of Cape Town electron microscopy unit using standard procedures.

Data Analysis. Analysis of the infrared data was carried out using linear least-squares fitting methods with the program GraphPad Prism. The data were fitted to eq 2:

$$\Delta A = \Delta A_\infty\{1 - \exp(-zt^n)\} \quad (2)$$

This involves substitution of eq 1 into the Avrami equation (*34*) (eq 3):

$$m/m_0 = \exp(-zt^n) \quad (3)$$

In the above equations, z is an empirical rate constant and n is a constant known as the Avrami constant, which is usually an integer ranging between 1 and 4. Where the reactions were seeded, the data were fitted to eq 4:

$$\Delta A = x\Delta A_\infty + (1 - x)\Delta A_\infty\{1 - \exp(-zt^n)\} \quad (4)$$

where x is the mass fraction of β-haematin added to the reaction mixture at the beginning of the reaction. In the plots, the data are displayed as $\%(\Delta A/\Delta A_\infty)$ vs time.

RESULTS

Identity of Reactants and Products. We have previously fully characterized (*32*) both the initial precipitate formed upon addition of acetate to a solution of hemin (under conditions identical to that used in this study) and the product obtained upon heating of this mixture at 60 °C for 30 min. Elemental analysis of the starting material was found to be identical with that expected for hematin (and clearly distinguishable from β-hematin). Infrared (*32*) and Mössbauer (*29*) spectra of the precipitate are completely consistent with this conclusion and further demonstrate that the initial precipitate is neither an acetate complex of Fe(III)PPIX [no evidence of an Fe(III)-coordinated carboxylate group in the IR spectrum] nor a μ-oxo dimer of Fe(III)PPIX (as the Mössbauer spectrum is not that of the dimer). On the other hand, the final product of the reaction has been conclusively shown to be β-hematin by X-ray diffraction and elemental analysis (*32*). We can thus confidently conclude that the process under observation in the current study corresponds to the conversion of hematin to β-hematin.

Infrared Spectroscopic Observation of β-Hematin Formation. Hematin and β-hematin can be distinguished by IR spectroscopy (*24*, *32*). Significant and characteristic changes in peak positions and in the sharpness of peaks are observed throughout the spectrum. The most intense peaks characteristic of β-hematin are seen in the vicinity of 1663 and 1210 cm^{-1}. These peaks are absent in hematin. The former peak is believed to arise from the C═O stretch of the carboxylate group coordinated to the Fe(III) center, while the latter arises from the C—O single bond stretch of the same group (*24*). We selected the peak at 1210 cm^{-1} as the most convenient for quantitative monitoring of the reaction because there is less overlap with neighboring peaks.

The dependence of ΔA_{1210} on the incubation time of hematin in 4.5 M acetate at pH 4.5 and 60 °C was determined by quenching, washing, and drying samples at specific time points and then measuring the infrared absorbance of the carefully weighed material as described under Materials and Methods. A sigmoidal dependence was observed as shown in Figure 2a. There is an induction period of about 15 min during which little reaction occurs, followed by a period of rapid reaction from about 15 min to 40 min after which the process is virtually complete. This sigmoidal kinetic profile can be interpreted either as a process involving nucleation and growth phases or as evidence of an autocatalytic reaction.

X-ray Diffraction. Since the infrared peak at 1210 cm^{-1} demonstrates the formation of an iron−carboxylate bond, but not necessarily the formation of the crystalline product corresponding to β-hematin, we repeated the experiment on a larger scale to obtain material at various reaction times for X-ray powder diffraction. Diffraction patterns of the dried product at various time points are shown in Figure 2b. Hematin exhibits two broad diffraction peaks. This can be interpreted as evidence either of a material containing crystallites considerably smaller than 200 nm (*35*), or of an amorphous solid which would typically be expected to contain a number of very broad diffraction humps (*36*). In the case of the first interpretation, an estimation of the size of crystallites from the extent of line broadening may be obtained from the Scherrer formula[2] (*35*). In the current case, the additional line broadening at half-peak height for the peak centered at 9.6° (compared to β-hematin whose average particle size is greater than 200 nm) is estimated to be about 0.060 ± 0.023 rad. This suggests a crystal size between about 20 and 44 Å. It is probably a matter of debate whether a material made up of such small regions of order represents

[2] Here crystal thickness, t (in Å), is given by the equation: $t = 0.9\lambda/(B \cos \theta)$, where λ is the wavelength of the X-rays in angstroms and θ is the Bragg angle. B is the line broadening obtained from the Warren formula: $B^2 = B_M^2 - B_S^2$, where B_M is the measured peak width in radians at the half-peak height and B_S is that of a nearby peak of a standard with a crystal size in excess of 200 nm which should be mixed in with the sample. In this case, B_S has been estimated from the nearby β-hematin peak obtained under identical conditions with the identical sample holder (and effectively mixed in at intermediate times).

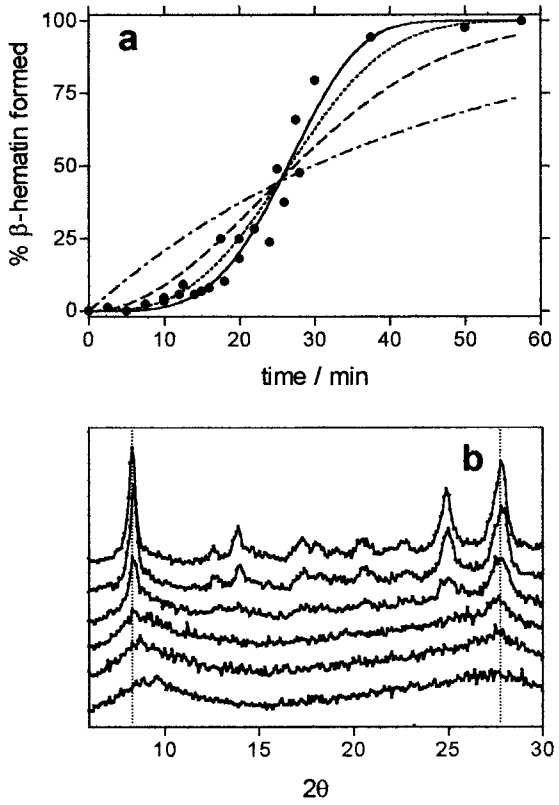

FIGURE 2: Time course (a) of β-hematin formation measured by IR spectroscopy (●). Times refer to the period of incubation in 4.5 M acetate, pH 4.5, 60 °C. The data represent a superimposition of three independent experiments. Lines are best fits of the data to the Avrami equation with (—) $n = 4$, (· · ·) $n = 3$, (– –) $n = 2$, and (– · –) $n = 1$. XRD patterns (b) of dried samples obtained from the reaction under the same conditions at (from bottom to top) 0, 5, 15, 20, 30, and 60 min. Co Kα radiation ($\lambda = 1.789$ Å). Vertical dotted lines at the positions of the two strongest peaks in β-hematin have been inserted to emphasize the fact that the broad peaks of hematin do not occur at the same 2θ values and thus do not arise from identical lattice spacings.

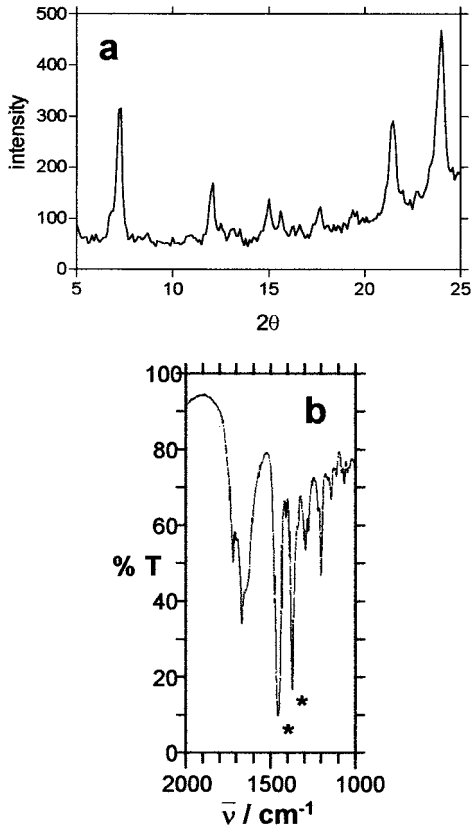

FIGURE 3: XRD pattern (a) of an undried product obtained after 60 min of reaction carried out under the same conditions as in Figure 2. The rising background seen above 20° (2θ) was found to reach a maximum intensity at approximately 30°. Note, Cu Kα radiation ($\lambda = 1.541$ Å) was used in this experiment. When this is taken into account, the diffraction pattern is found to be identical to that of dried β-hematin. IR spectrum (b) of the same material obtained as a Nujol mull. Peaks marked with an asterisk are due to Nujol. The most prominent peaks occur at 1710, 1661, 1299, and 1211 cm^{-1}.

a truly crystalline solid or an amorphous material. The diffraction pattern of hematin is significantly different from that of β-hematin not only with respect to the widths of the diffraction peaks but also with respect to their positions. Combined with elemental analysis and spectroscopic evidence presented previously (*29*, *32*) these changes in the diffraction pattern can be ascribed to a conversion of one solid substance into another.

The time dependence of changes in the diffraction pattern corresponds closely to the IR observations. After 5 min of reaction, the largest diffraction peaks of β-hematin are not yet clearly discernible on the broad background pattern of hematin. At 15 min, these peaks are barely discernible, but by 20 min the characteristic diffraction pattern of β-hematin (*5*, *32*) is easily seen. Rapid growth of the diffraction pattern occurs during the period 15−30 min. No change in the diffraction pattern occurs after 60 min, even if the process is allowed to continue for 24 h (not shown). In addition to the growth of the β-hematin diffraction peaks during the reaction, the pattern arising from the starting material disappears during the process, with the broad peaks decreasing until the baseline becomes virtually flat by the end of the process. This indicates that hematin is largely converted to product. This accords with our previous findings using elemental analysis (*32*) which suggest almost complete conversion and contrasts with a number of reports based on differential solubilization in carbonate or DMSO solution which suggested that reaction products formed in more acidic acetate solutions are only about 50% β-hematin (*24*, *26*).

Analysis of Undried Products. Recently it has been suggested that the formation of β-hematin does not occur during the incubation of hematin at pH 4.5 in 4.5 M acetate, but rather during drying of the washed product over P_2O_5 (*33*). We have therefore determined the XRD pattern of the wet product at the end of the reaction (Figure 3a). The diffraction pattern is identical to that of dry β-hematin except for a broad peak centered near a 2θ value of approximately 30°. This corresponds closely to the radial distribution function of oxygen atoms in liquid water (approximately 2.9 Å) (*37*). The diffraction pattern shows unequivocally that β-hematin is formed during the acetate incubation process. An IR spectrum of the product obtained as a Nujol mull (Figure 3b) is also virtually identical to that of the dried product in all observable peaks (*32*). IR spectra obtained as Nujol mulls are unsuited to quantitation, and the amounts of material used in the XRD analysis also make accurate quantitation impractical. As a result, these observations themselves cannot preclude the possibility that additional β-hematin may be formed during the drying process. However, we can infer that this is not the case from our

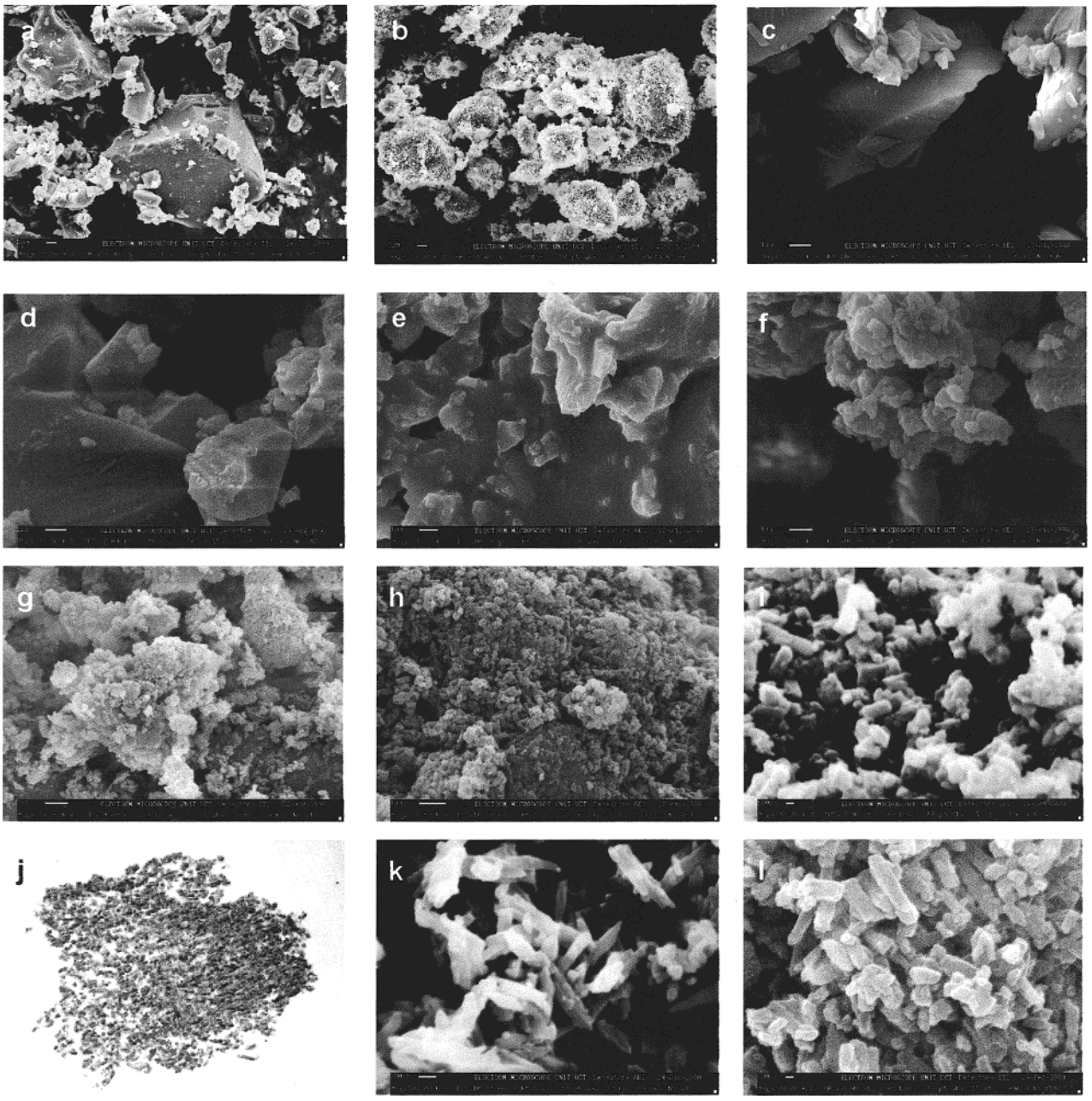

FIGURE 4: Scanning electron micrographs of dried samples obtained at (a) 0, (b) 60, (c) 0, (d) 5, (e) 15, (f) 20, (g) 30, (h) 60, and (i) 60 min reaction under the same conditions as in Figure 2. A transmission electron micrograph (j) of a thin section of the product obtained after 60 min reaction. Material prepared (k) in 8.5 M acetate, pH 4.5, 60 °C, and obtained at 60 min reaction time. Product (l) obtained after 150 min reaction in 4.5 M acetate, pH 4.5, 60 °C, unstirred. Scales: (a and b) 535:1, (c) 3533:1, (d) 3466:1, (e) 2912:1, (f) 3641:1, (g) 3586:1, (h) 4184:1, (i and l) 13843:1, (j) 4293:1, and (k) 14160:1 as published.

observations on the dried material. The reaction times shown in Figure 2a correspond to the duration of incubation in acetate solution. The drying process, on the other hand, was carried out over arbitrary periods of time equal to or exceeding 48 h at room temperature. If significant additional β-hematin formation were to occur during this process, either no dependence on incubation time would be observed, or large and random errors would be introduced into the data.

Electron Microscopy. To observe the changes in external appearance of these materials during the reaction, we performed SEM on the dried products. At relatively low magnification, hematin is seen to consist of large angular particles ranging from about 3 to 50 μm in size (Figure 4a). It would appear that during the course of the reaction these large particles persist, but undergo a transformation in their external appearance (Figure 4b). At higher magnification, the particles of hematin are revealed to have a smooth surface (Figure 4c). Despite the fact that these relatively large hematin particles superficially appear to be crystals, the XRD data described above show it to be essentially amorphous. Observation of the surface of hematin at the highest available magnification (100000×, not shown) indicates that it is perfectly smooth at this resolution, and so any crystals that may be present are smaller than about 30 nm (in agreement with the XRD data which indicate that any possible crystallites present are about an order of magnitude smaller than this). The particles of hematin observed at lower magnification exhibit concoidal fractures like glass. By the end of the reaction, the previously smooth surface has changed into a mass of small, but clearly discernible crystals (typically about

150−350 nm long) (Figure 4h,i). The appearance of the surface at intermediate times is consistent with the IR and XRD observations. After 5 min of reaction (Figure 4d), no observable change occurs. At 15 min, small bumps become visible on the surface (Figure 4e), while after 20 min a major change in the surface is underway (Figure 4f), with small crystals clearly distinguishable after 30 min (Figure 4g). At 60 min, the entire surface appears to consist of small crystals with no evidence of the original starting material, or any other particles. This is again consistent with the almost complete conversion of the material to β-hematin. No further change is observed if the incubation is continued for 24 h. As SEM shows only the surface of the solid, we had the final reaction product embedded in resin and cut into thin sections. TEM of the thin sections reveals that the large particles are transformed throughout their interior (Figure 4j). This shows that the change is not merely a surface phenomenon.

Quantitative Modeling of β-Hematin Formation. The Avrami equation (eq 3) is commonly used to model many different solid-state processes that involve nucleation and growth. These include crystal decomposition reactions (*38*), polymer crystallization (*34*), and mineral crystallization processes (*39*). An exact description of such a process is mathematically difficult, because the geometry of the growth process may be complex and because of the problem of impingement that occurs when the growing solid nucleated at one site meets that nucleated at another. The Avrami equation is an approximate solution to this problem (*34*). In the Avrami equation, the value of n is a function of the dimensionality of the growth process (assumed to be spherical, circular, or linear) and the type of nucleation (instantaneous or sporadic). The value of n is often found to be an integer ranging between 1 and 4, although nonintegral values lying between these limits are sometimes observed (*34*). The observed rate constant, z, is related to the rate constants for nucleation (N) and linear growth along each Cartesian axis (G). In the case of spherical growth and first-order nucleation ($n = 4$), the relationship is given by eq 5:

$$z = 4\pi NG^3\rho_p/3\rho_r \quad (5)$$

Here ρ_p is the density of product and ρ_r is the density of reactant.

Since both the XRD and SEM data indicate that the process revealed by monitoring the growth of the infrared band at 1210 cm^{-1} involves not only formation of cyclic Fe(III)PPIX dimers which make up β-hematin, but also its crystallization, we chose to interpret the sigmoidal kinetics as evidence of a process of nucleation and growth (as indicated below, the alternative hypothesis of an autocatalytic reaction was specifically discounted). For this reason, we elected to fit the data to the Avrami equation. When the data for β-hematin formation at 60 °C in 4.5 M acetate, pH 4.5, were fitted to this equation, the value of n was found to be close to 4 (see Table 1). The standard deviation in the value of z was found to be large when both n and z were permitted to refine freely, and this was traced to a strong correlation between these parameters, which is inherent in the form of the mathematical function. Since the standard deviation in n is relatively small, it is possible to obtain a fitted value of n and then optimize z with n fixed. This results in acceptable standard deviations in z. Our procedure was to fix n to the nearest integer to the fitted value and then to separately optimize z. Best fits to the Avrami equation for data obtained at pH 4.5 in 4.5 M acetate at 60 °C are shown in Figure 2a. It is clear that values of $n = 1$ or 2 are untenable, but the choice between $n = 3$ or 4 is less obvious. When the residuals were plotted, however, it was immediately apparent that systematic deviations occur with $n = 3$, but not with $n = 4$. Thus, $n = 4$ appears to most closely model the data under these conditions. The growth geometry thus approximates to the spherical case with sporadic nucleation (i.e., nucleation occurring at a constant rate).

Table 1: Rate Constants (z) and Avrami Constants (n) Obtained by Nonlinear Least-Squares Fitting of the Data to Equation 2 (Standard Stirring Rate, except Where Otherwise Indicated)

temp (°C)	[acetate] (M)	pH	n(fitted)[a]	n(fixed)	z[a] (min^{-n})
60[b]	4.5	4.5	4.3 ± 0.6	4	$(1.2 \pm 0.1) \times 10^{-6}$
60[c,d]	4.5	4.5	3.3 ± 0.4	3	$(6.4 \pm 0.7) \times 10^{-6}$
60[e]	4.5	4.5	2.4 ± 0.2	2	$(1.7 \pm 0.2) \times 10^{-4}$
50[b]	4.5	4.5	4.3 ± 0.3	4	$(2.2 \pm 0.1) \times 10^{-8}$
37[f]	4.5	4.5	4.38 ± 0.01	4	$(2.3 \pm 0.2) \times 10^{-10}$
30[g]	4.5	4.5	−	4	$(6.0 \pm 0.7) \times 10^{-12}$
60	2.0	4.5	3.8 ± 0.5	4	$(1.7 \pm 0.3) \times 10^{-9}$
60	3.5	4.5	3.3 ± 0.1	3	$(3.1 \pm 0.6) \times 10^{-6}$
				4	$(5.3 \pm 3.3) \times 10^{-8}$
60	5.5	4.5	2.94 ± 0.05	3	$(3.0 \pm 0.7) \times 10^{-5}$
60	7.0	4.5	2.3 ± 0.5	2	$(1.44 \pm 0.09) \times 10^{-3}$
60	8.5	4.5	2.2 ± 0.2	2	$(3.3 \pm 0.9) \times 10^{-3}$
60	4.5	2.5	4.2 ± 0.1	4	$(1.2 \pm 0.4) \times 10^{-8}$
60	4.5	3.0	2.8 ± 0.3	3	$(6.4 \pm 1.1) \times 10^{-5}$
60[h]	4.5	3.5	2.9 ± 0.3	3	$(1.3 \pm 0.1) \times 10^{-4}$
60[i]	4.5	4.0	3.4 ± 0.4	3	$(1.06 \pm 0.04) \times 10^{-4}$
			3.9 ± 0.3	4	$(2.4 \pm 0.1) \times 10^{-6}$
60[h]	4.5	5.0	3.3 ± 0.1	3	$(1.7 \pm 0.4) \times 10^{-7}$
50[j,d]	4.5	4.5	3.5 ± 0.2	4	$(4.7 \pm 0.3) \times 10^{-8}$
50[k]	4.5	4.5	−	4	$(4.5 \pm 0.7) \times 10^{-8}$
60[j]	8.5	4.5	2.0 ± 0.2	2	$(2.7 \pm 0.7) \times 10^{-3}$

[a] Maximum deviation for two independent measurements except where otherwise stated. [b] Data for three independent measurements combined; errors are standard deviations obtained from the fitting procedure. [c] Stirred at half the normal rate. [d] Single determination; errors are standard deviations obtained from the fitting procedure. [e] No stirring. [f] Data for two independent experiments combined; errors are standard deviations from the fitting procedure. [g] Data for two independent experiments combined; n fixed at 4.0 gives $r^2 = 0.98$. [h] Mean for three independent experiments ± standard error of mean. [i] Two independent experiments giving rise to different values of n. [j] Seeded with 10% β-hematin. [k] Seeded with 50% β-hematin; n fixed at 4.0 gives $r^2 = 0.90$.

Effect of Stirring Rate. When the reaction is carried out unstirred, or at half the normal stirring rate, there are profound changes, with a large change in the rate constant and a change in the value of the Avrami constant (Table 1, Figure 5a). This does not, however, imply that the reaction is not reproducible. Consistent results are obtained provided that all conditions, including stirring rate, total volume, vessel dimensions, acetate concentration, pH, and temperature, are carefully controlled and rigorously reproduced. We also found that if an aged stock solution of hemin in NaOH (16 h) was used in the reaction, no β-hematin formation occurred. It is well established that Fe(III)PPIX solutions oxidize over a period of hours in basic solution (*40*), and it is therefore essential to use fresh hemin for all reactions.

Effect of Temperature. When the reaction is carried out at lower temperatures (50, 37, or 30 °C), the rate decreases

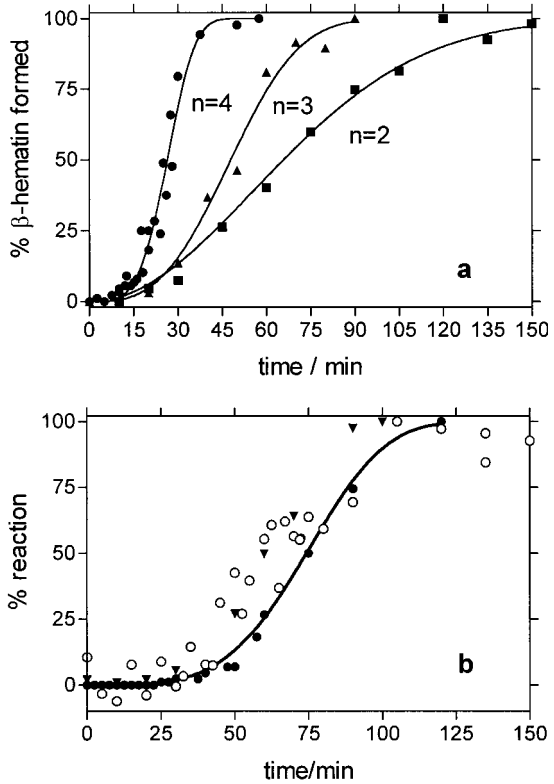

FIGURE 5: Time course (a) of β-hematin formation under the conditions described in Figure 2 with (●) stirring at the normal rate (150 ± 10 rpm), (▲) half the normal rate (75 ± 10 rpm), and (■) unstirred. The values of n refer to the integer values of the Avrami constant that best model the data. Formation of β-hematin (b) in 4.5 M acetate, pH 4.5 at 50 °C: (●) unseeded, (▼) seeded with 10% β-hematin, and (○) seeded with 50% β-hematin. Plots normalized to show fraction of total change.

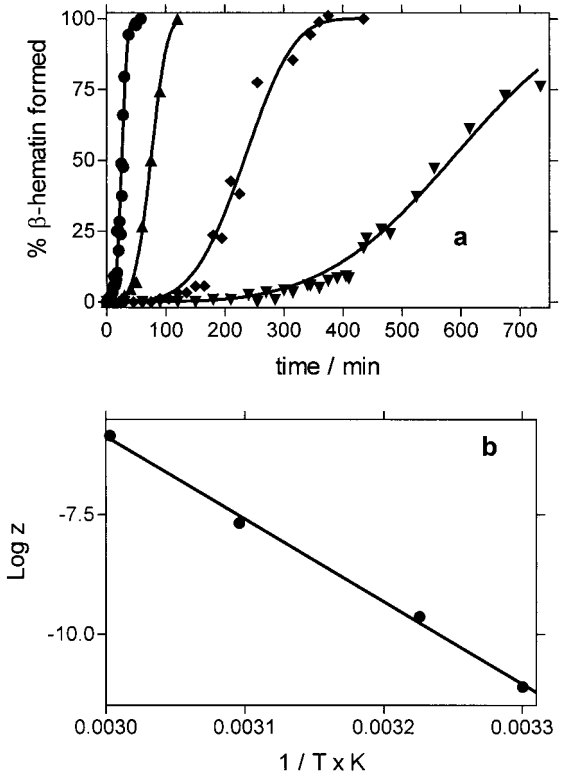

FIGURE 6: Effect of temperature (a) on β-hematin formation in 4.5 M acetate, pH 4.5, at (●) 60, (▲) 50, (◆) 37, and (▼) 30 °C. Solid lines represent a best fit of the data to the Avrami equation with $n = 4$. Plots for 60 and 50 °C show three data sets combined, while two data sets are combined in the plots at 37 and 30 °C. Arrhenius plot (b) of the rate constants (z) obtained by fitting the data shown in panel a to the Avrami equation with $n = 4$.

substantially, with a corresponding increase in the induction phase (Figure 6a). The kinetic traces still conform to an Avrami constant of 4 (see Table 1). The rate constants conform closely to the Arrhenius equation (Figure 6b), indicating an activation energy of 331 ± 13 kJ/mol. This value shows that there is a considerable activation barrier in this process. The close conformity of the data to the Arrhenius equation strongly supports the data analysis approach used and provides further evidence that the reaction occurs entirely during the acetate incubation process.

Effect of Acetate Concentration. Acetate concentration was found to have a profound influence on reaction rates (Figure 7). In 2.0 and 3.5 M acetate at pH 4.5 and 60 °C, the induction and growth phases of the process are much slower (Table 1 and Figure 7a). The induction phase lasts for more than an hour in 2.0 M acetate, and the reaction takes almost 5 h to reach completion. The Avrami constant appears to be 4 under these conditions, although due to data scatter there is some ambiguity as to whether the value is 3 or 4 in 3.5 M acetate. When the acetate concentration is 5.5, 7.0, or 8.5 M, the time required for the reaction to reach completion is much the same as in 4.5 M acetate (Figure 7b). The shape of the reaction profile changes, however, and there is a change in the value of the Avrami constant to 3 in 5.5 M acetate and to 2 in 7.0 and 8.5 M acetate (Table 1). The product obtained in 8.5 M acetate has an identical XRD pattern to β-hematin formed in 4.5 M acetate, demonstrating that it is structurally and chemically identical. SEM and TEM, however, appear to reveal some change in the external appearance of the crystals. They are somewhat larger and more needlelike (about 450−750 nm long) (Figure 4k). Indeed, they appear very similar to crystals of natural hemozoin (*32*). Material isolated from the reaction performed in 4.5 M acetate without stirring, where n is also 2, is very similar (Figure 4l), and this suggests that changes in the value of n in this system may correlate with observable changes in the size and external appearance of the crystals. There is a strong dependence of rate constant on acetate concentration (Table 1), and it appears that the nth root of z may have a linear dependence on acetate concentration (Figure 7a, inset). This seems to suggest that the nucleation and linear growth rate constants N and G each have a first-order dependence on acetate concentration. This cannot, however, be confirmed from the current data because of the changes in the value of n as acetate concentration increases. The relationship between z, N, and G differs for different values of n (because of differences in the geometry of crystal growth), and so rate constants at many more acetate concentrations (where n is fixed) would be required to definitively determine the quantitative dependence of z on acetate concentration.

Effect of pH. Variations in pH with acetate fixed at 4.5 M and temperature at 60 °C cause a considerable change in the rate of reaction with an apparent maximal rate around pH 3.5. Fitted values of n generally lie between 3 and 4 (Table 1). These differences in n may in part be due to data scatter, but the shapes of the reaction profiles in many cases show that there are genuine differences in the n value. This

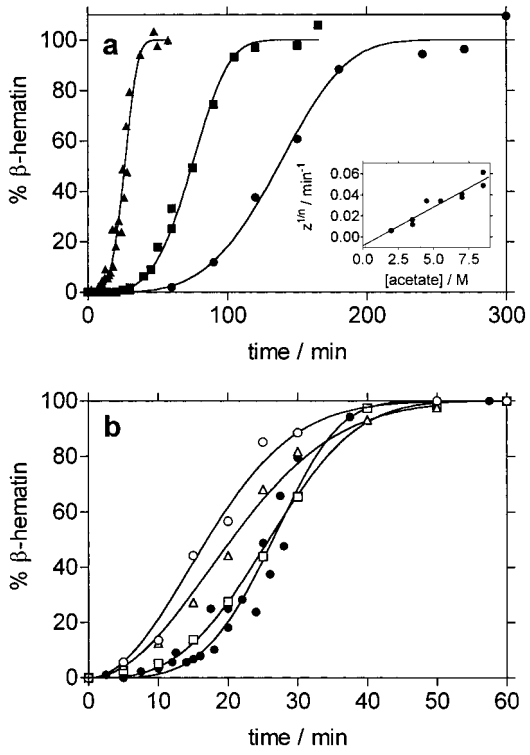

FIGURE 7: Effect of acetate concentration (a) on β-hematin formation at pH 4.5 and 60 °C: (●) 2.0, (■) 3.5, and (▲) 4.5 M. Solid lines represent a best fit of the data to the Avrami equation with $n = 4$. Effect of acetate concentration (b) under the same conditions: (●) 4.5, (□) 5.5, (△) 7.0, and (○) 8.5 M. Solid lines represent best fits of the data to the Avrami equation with (●) $n = 4$, (□) $n = 3$, and (△, ○) $n = 2$. Inset on panel a: plot of the nth root of the rate constants ($z^{1/n}$) versus molar concentration of acetate for the data shown in panels a and b.

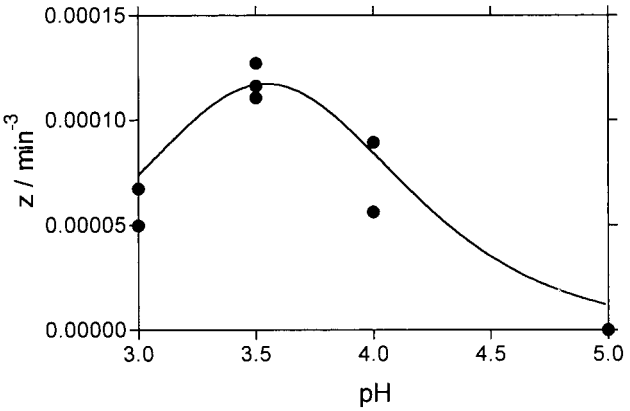

FIGURE 8: Plot of the rate constants (z) obtained from best fits of the data to the Avrami equation where $n = 3$ as a function of pH. The solid line was drawn using a function that describes two protonation equilibria and assumes that only the monoprotonated species reacts at an appreciable rate where the fraction of monoprotonated species is given by: $1/\{(K_{a2}/[H^+]) + ([H^+]/K_{a1}) + 1)\}$. The p$K_a$ values used (3.5 and 3.6) were chosen for graphic display only and do not represent genuine fits to the data.

change in the Avrami constant makes it difficult to compare some of the data at different pH values. Most of the data points conform to $n = 3$, and a plot of the rate constants for just these points clearly indicates a bell-shaped dependence on pH, with slower reactions at pH 3.0 and at pH 5.0, but a maximal rate at pH 3.5 (Figure 8). This accords with other evidence reported in the literature (*13*, *21*, *31*) indicating a similar type of pH dependence and that suggests maximal yields around pH 3.5 (*31*). The data are consistent with an equation that assumes two protonation sites, with only the monoprotonated species reacting at an appreciable rate. Although the pK_a values of these protonation equilibria can in principle be extracted from the data, the magnitude of scatter and the relatively small number of data points preclude it in this case.

Effect of Seeding. The sigmoidal time dependence of β-hematin formation could be ascribed to an autocatalytic reaction. To test this possibility, we performed the reaction in 4.5 and 8.5 M acetate after seeding the reactants with 10 or 50% β-hematin. This had a negligible effect on the rate of reaction (Figure 5b) and confirms our previously reported observation (*29*). The increase in rate constant was barely statistically significant (Table 1). The reaction is thus not autocatalytic under these conditions.

DISCUSSION

Several characteristics of β-hematin formation revealed in this work probably account for previously reported disputes over the conditions under which it forms (*14*, *29*−*33*). The infrared data clearly show that the reaction follows a sigmoidal growth path, and this is qualitatively confirmed by both XRD and SEM. This finding is in accord with a previous report by Dorn et al. (*21*), but is at odds with our previous Mössbauer evidence (*29*). This can probably be ascribed to the magnitude of the standard errors in our earlier study (*29*), which may have masked the sigmoidal shape of the curve. The current data also show that rates of β-hematin formation are strongly dependent on stirring rate. This suggests that it is probably very difficult to reproduce the same reaction rates in different laboratories. Indeed, it is likely that reactions previously observed by various groups occurred at significantly different rates, even where conditions other than stirring rate were quite similar. As a result, where β-hematin formation was observed only after a fixed time interval, it is possible that in some cases the reaction was still in the induction phase, and the conclusion was reached that no reaction occurs. In other cases, only a slightly faster reaction rate would have resulted in the material having passed through the growth phase, and an opposite conclusion would have been reached. This problem is exacerbated by an approximately fourth-order dependence on acetate concentration (in 4.5 M acetate), a strong dependence on pH and temperature, and sensitivity of hematin to oxidation in basic solution. Our results unequivocally demonstrate that the reaction occurs in 4.5 M acetate at pH 4.5 during the incubation, rather than drying stage, and there is no apparent evidence of a build-up of any intermediate species. We have noticed, however, that the infrared spectrum of hematin (but not β-hematin) undergoes changes upon drying. In Nujol mulls of the wet hematin, the IR spectrum shows broad unresolved peaks in the range 1717−1617 cm^{-1}, and a maximum intensity is observed around 1638 cm^{-1}. This is probably due to hydrogen bonding of water to the hematin carboxylate/carboxylic acid groups, which is absent in the dry material. We suspect that a material previously described as B-hematin (*31*, *33*) may in fact be a mixture of partially hydrated hematin and β-hematin.

Comparison of the IR, XRD, and SEM results shows that formation of the Fe(III)−carboxylate bond and formation of the crystalline product are essentially simultaneous. There

is no evidence that the dimers that make up β-hematin are formed in a discreet process before crystallization occurs. The process of β-hematin formation can thus be thought of as partly a crystallization process. It proceeds by rapid precipitation of amorphous (or possibly nanocrystalline) hematin, followed by slow conversion to crystalline β-hematin. The dependence on both stirring rate and acetate concentration suggests that this happens via dissolution of the initial hematin solid and reprecipitation as β-hematin. We have previously shown (*14*) that acetate solubilizes hematin in acidic solution, and there is an indication in the current data (see Results) that both the nucleation and linear growth rates of β-hematin may have a first-order dependence on acetate concentration. Both of these effects could be explained by the formation of a soluble heme−acetate complex as described by eq 6:

$$H_2O{-}Fe(III)PPIX(s) + AcO^-(aq) \rightleftharpoons AcO{-}Fe(III)PPIX^-(aq) + H_2O(l) \quad (6)$$

The concentration of this acetate complex would have a first-order dependence on free acetate concentration, and it may be this species that both reacts to form β-hematin nuclei and reacts with the growing crystal, with acetate thus acting as a phase transfer catalyst as we have previously suggested (*29*). The lack of effect of seeding suggests that there is negligible transport of hematin through the bulk medium, but that dissolution and reprecipitation occur within the relatively large particles which can be observed in low-magnification SEM (Figure 4a,b). Stirring probably plays a role in assisting removal of water from these particles by agitating the surface interface of the particles. If this water is not efficiently removed, it is likely that the acetate concentration within spaces inside these particles would decline due to dilution, slowing the reaction. The pH dependence of the process is readily explained on the basis of the protonation state of β-hematin itself, where each Fe(III)PPIX is monoprotonated. It would appear that only the corresponding species of hematin reacts to form β-hematin, and so at low pH (<2), where the diprotonated species is predominant, and at higher pH (>5,) where the unprotonated species is dominant, the reaction is slow. It is possible that two other factors may also contribute to the bell-shaped dependence on pH. Formation of μ-oxo dimers of hematin at the higher end of the range could be expected to slow β-hematin formation, while the decrease in concentration of free acetate ion at lower pH may also contribute to slower reaction under these conditions.

The process of β-hematin formation described above closely parallels many mineral formation processes which occur by rapid precipitation of the most soluble solid (often amorphous), followed by slow conversion to increasingly less soluble, but thermodynamically more stable solids (*41*). Interconversion of the solids is believed to occur via dissolution and reprecipitation and is dependent on the presence of a solvent. This behavior is referred to as Ostwald's rule of stages and is illustrated by the in vitro formation of hydroxyapatite. In acidic solution, this occurs (*41*) via rapid precipitation of amorphous calcium phosphate which then converts to less soluble dicalcium phosphate dihydrate and finally to even less soluble hydroxyapatite. The formation of β-hematin differs only inasmuch as the inner coordination sphere of the Fe(III) ion undergoes a change, with loss of water and replacement by the propionate group of a neighboring Fe(III)PPIX. Even though the loss of coordinated water is a dehydration process occurring in an aqueous milieu, it is not unusual for Fe(III)PPIX. A similar dehydration reaction occurs in dilute solution during formation of the μ-oxo dimer.

On the basis of this evidence, we can envisage two possible models to account for hemozoin formation in vivo. If the release of heme from hemoglobin is so fast that the concentration of hematin exceeds its solubility limit, it will precipitate. The process is then likely to proceed in a manner similar to that in acetate solution. In this case, some compound or compounds would have to play a role analogous to acetate, but at much lower concentration. We have found preliminary evidence that some carboxylates are much more active than acetate. For example, benzoic acid appears to promote β-hematin formation at about one-fiftieth of the concentration of acetate at the same pH and temperature. There are also indications (*21*, *22*) that lipids could play a role in the process. If the process in vivo occurs in this way, it is difficult to imagine that proteins would be able to penetrate into the solid particles of hematin, and it is also unlikely that preexisting hemozoin would influence reaction rates, as our results show that β-hematin seems to have little effect in vitro under these conditions. If, on the other hand, the release of heme from hemoglobin is carefully controlled never to exceed the solubility limit of hematin, but it is supersaturated with respect to β-hematin, it may potentially form hemozoin directly from solution provided a suitable nucleation site is available. There is considerable evidence that histidine-rich protein II (HRPII) promotes hemozoin formation (*23*). This remarkable protein has been shown to bind 50 Fe(III)PPIX molecules, probably as low-spin bis-histidyl complexes (*42*), and a dendrimer containing its repeat sequence has been shown to produce β-hematin (*43*). HRPII may also weakly bind Fe(III)PPIX to aspartate groups on its surface (*44*) at low pH. The carboxylate groups of Fe(III)PPIX bound to HRPII might act as a nucleation site for β-hematin formation, possibly by behaving as an epitaxial growth surface, or stabilizing β-hematin nuclei. Such a process would be analogous to that proposed for the formation of hydroxyapatite in bone crystal which appears to form directly from solution without precipitation of amorphous calcium phosphate (*41*) and which has been suggested to occur epitaxially on the surface of collagen (*45*). This notion that hemozoin formation occurs under careful biological control and by interaction with a protein matrix is appealing and is in accord with what is commonly observed in biomineralization processes (*46*). Experiments aimed at detecting whether large quantities of precipitated hematin are present in the parasite should be able to distinguish between these two models.

CONCLUSION

In conclusion, new evidence relating to the process of β-hematin formation reported here together with the recent solution of its crystal structure (*20*) indicate that the formation of hemozoin should be viewed in light of the paradigm of biomineralization. It is our view that the ideas relating to biomineralization processes are more appropriate to under-

standing hemozoin formation than the concepts of polymer formation, or of conventional chemical or biochemical reactions. According to this view, antimalarials such as chloroquine could be seen as crystallization inhibitors, which by inhibiting β-hematin crystallization favor formation of an alternative form, namely, hematin. The fact that chloroquine inhibits hemozoin formation at substoichiometric concentrations (*20*) suggests that this could occur via blocking of the smallest, but fastest growing face of the crystal, as has been proposed by Pagola et al. (*20*). Alternatively, it could occur by inhibition of the nucleation process itself, a common method of control in biomineralization processes (*41*). Both of these proposals would seem to be in accord with earlier observations which had been interpreted as evidence of capping of a growing polymer chain (*16*).

ACKNOWLEDGMENT

We thank Prof. Mino Caira and Mr. Vincent Smith of the Department of Chemistry, University of Cape Town, for assistance with the XRD analysis.

REFERENCES

1. World Health Organization Report on Infectious Diseases, Removing Obstacles to Healthy Development, WHO, Geneva (1999).
2. Rudzinska, M. A., Trager, W., and Bray, R. S. (1965) *J. Protozool. 12*, 563−576.
3. Ladan, H., Nitzan, Y., and Malik, Z. (1993) *FEMS Microbiol. Lett. 112*, 173−177.
4. Scheibel, L. W., and Sherman, I. W. (1988) *Malaria: Principles and Practice of Malariology* (Wernsdorfer, W. H., and McGregor, I., Eds.) pp 219−252, Churchill-Livingstone, Edinburgh.
5. Bohle, D. S., Dinnebier, R. E., Madsen, S. K., and Stephens, P. W. (1997) *J. Biol. Chem. 272*, 713−716.
6. Mungthin, M., Bray, P. G., Ridley, R. G., and Ward, S. A. (1998) *Antimicrob. Agents Chemother. 42*, 2973−2977.
7. Bray, P. G., Mungthin, M., Ridley, R. G., and Ward, S. R. (1998) *Mol. Pharmacol. 54*, 170−179.
8. Ginsburg, H., Famin, O., Zhang, J., and Krugliak, M. (1998) *Biochem. Pharmacol. 56*, 1305−1313.
9. Loria, P., Miller, S., Foley, M., and Tilley, L. (1999) *Biochem. J. 339*, 363−370.
10. Bray, P. G., Janneh, O., Raynes, K. J., Mungthin, M., Ginsburg, H., and Ward, S. A. (1999) *J. Cell Biol. 145*, 363−376.
11. Vippagunta, S. R., Dorn, A., Matile, H., Bhattacharjee, A. K., Karle, J. M., Ellis, W. Y., Ridley, R. G., and Vennerstrom, J. L. (1999) *J. Med. Chem. 42*, 4630−4639.
12. Egan, T. J., Hunter, R., Kaschula, C. H., Marques, H. M., Misplon, A., and Walden, J. (2000) *J. Med. Chem. 43*, 283−291.
13. Slater, A. F. G., and Cerami, A. (1992) *Nature 355*, 167−169.
14. Egan, T. J., Ross, D. C., and Adams, P. A. (1994) *FEBS Lett. 352*, 54−57.
15. Dorn, A., Stoffel, R., Matile, H., Bubendorf, A., and Ridley, R. G. (1995) *Nature 374*, 269−271.
16. Sullivan, D. J., Gluzman, I. Y., Russel, D. G., and Goldberg, D. E. (1996) *Proc. Natl. Acad. Sci. U.S.A. 93*, 11865−11870.
17. Hawley, S. R., Bray, P. G., Mungthin, M., Atkinson, J. D., O'Neill, P. M., and Ward, S. A. (1998) *Antimicrob. Agents Chemother. 42*, 682−686.
18. Dorn, A., Vippagunta, S. R., Matile, H., Jaquet, C., Vennerstrom, J. L., and Ridley, R. G. (1998) *Biochem. Pharmacol. 55*, 727−736.
19. Sullivan, D. J., Matile, H., Ridley, R. G., and Goldberg, D. E. (1998) *J. Biol. Chem. 273*, 31103−31107.
20. Pagola, S., Stephens, P. W., Bohle, D. S., Kosar, A. D., and Madsen, S. K. (2000) *Nature 404*, 307−310.
21. Dorn, A., Vippagunta, S. R., Matile, H., Bubendorf, A., Vennerstrom, J. L., and Ridley, R. G. (1998) *Biochem. Pharmacol. 55*, 737−747.
22. Ridley, R. G., Dorn, A., Matile, H., and Kansy, M. (1995) *Nature 378*, 138−139.
23. Sullivan, D. J., Gluzman, I. Y., and Goldberg, D. E. (1996) *Science 271*, 219−222.
24. Slater, A. F. G., Swiggard, W. J., Orton, B. R., Flitter, W. D., Goldberg, D. E., Cerami, A., and Henderson, G. B. (1991) *Proc. Natl. Acad. Sci. U.S.A. 88*, 325−329.
25. Basilico, N., Monti, D., Olliaro, P., and Taramelli, D. (1997) *FEBS Lett. 409*, 297−299.
26. Basilico, N., Pagani, E., Monti, D., Olliaro, P., and Taramelli, D. (1998) *J. Antimicrob. Chemother. 42*, 55−60.
27. Bohle, D. S., and Helms, J. B. (1993) *Biochem. Biophys. Res. Commun. 193*, 504−508.
28. Berger, B. J., Bendrat, K., and Cerami, A. (1995) *Anal. Biochem. 231*, 151−156.
29. Adams, P. A., Egan, T. J., Ross, D. C., Silver, J., and Marsh, P. J. (1996) *Biochem. J. 318*, 25−27.
30. Pandey, A. V., and Tekwani, B. L. (1996) *FEBS Lett. 393*, 189−192.
31. Blauer, G., and Akkawi, M. (1997) *J. Inorg. Biochem. 66*, 145−152.
32. Egan, T. J., Hempelmann, E., and Mavuso, W. W. (1999) *J. Inorg. Biochem. 73*, 101−107.
33. Blauer, G., and Akkawi, M. (2000) *Biochem. J. 346*, 249−250.
34. Sharples, A. (1966) *Introduction to Polymer Crystallization*, Edward Arnold, London.
35. West, A. R. (1987) in *Solid State Chemistry and its Applications*, pp 173−175, Wiley, Chichester.
36. West, A. R. (1987) in *Solid State Chemistry and its Applications*, p 52, Wiley, Chichester.
37. Narten, A. H., Danford, M. D., and Levy, H. A. (1967) *Discuss. Faraday Soc. 43*, 97−107.
38. Tompkins, F. C. (1976) in *Treatise on Solid State Chemistry* (Hannay, N. B., Ed.) Vol. 4, pp 193−231, Plenum Press, New York.
39. Kretz, R. (1994) *Metamorphic Crystallization*, Chapter 4, pp 263−329, John Wiley and Sons, Chichester.
40. Brown, S. B., Jones, P., and Suggett, A. (1968) *Trans. Faraday Soc. 64*, 986−993.
41. Kaim, W., and Schwederski, B. (1994) *Bioinorganic Chemistry: Inorganic Elements in the Chemistry of Life, an Introduction and Guide*, Chapter 15, John Wiley and Sons, Chichester.
42. Choi, C. Y. H., Cerda, J. F., Chu, H.-A., Babcock, G. T., and Marletta, M. A. (1999) *Biochemistry 38*, 16916−16924.
43. Ziegler, J., Chang, R. T., and Wright, D. W. (1999) *J. Am. Chem. Soc. 121*, 2395−2400.
44. Lynn, A., Chandra, S., Malhotra, P., and Chauhan, V. S. (1999) *FEBS Lett. 459*, 267−271.
45. Glimcher, M. J. (1984) *Philos. Trans. R. Soc. London, Ser. B B304*, 479−508.
46. Lowenstam, H. A., and Weiner, S. (1989) *On Biomineralization*, Oxford University Press, New York.

BI0013501